RSC Advances

PAPER

View Article Online
View Journal | View Issue

Cite this: *RSC Adv.*, 2023, **13**, 11393

Immobilized Ni on TMEDA@βSiO$_2$@αSiO$_2$@Fe$_3$O$_4$: as a novel magnetic nanocatalyst for preparation of pyrido[2,3-*d*:6,5-*d*′]dipyrimidines†

Yasir Qasim Almajidi,[a] Mohd Ubaidullah,*[b] Bidhan Pandit,[c] A. K. Kareem,[d] Rosario Mireya Romero-Parra,[e] Adizov Bobirjon,[f] Wesam R. Kadhum,[g] Amran M. AL-Erjan,[h] Munther Abosaooda[i] and Aisha Kamal Mahmoud[j]

In the current body of research, a very quick and effectual procedure for the synthesis of pyrido[2,3-*d*:6,5-*d*′]dipyrimidines has been developed. This method is accomplished through the one-pot multi-component reaction of 2-thiobarbituric acid, NH_4OAc and aldehydes utilizing Ni-TMEDA@βSiO$_2$@αSiO$_2$@Fe$_3$O$_4$ as a novel mesoporous nanomagnetic catalyst at room temperature. This protocol is one of the few reports of the preparation of these derivatives without the use of conventional heating as well as energies such as microwave and ultrasound radiation. The characterization of the prepared catalyst was well accomplished by different techniques such as FT-IR, ICP-OES, SEM, TEM, BET, XRD, VSM, TGA, EDX and Elemental mapping. This organometallic catalyst was reusable for seven times with negligible decrement in its catalytic performance. In addition, all of the products were produced with high TON and TOF values, which demonstrates that our catalyst has a very high level of activity in the preparation of pyrido[2,3-*d*:6,5-*d*′]dipyrimidines.

Received 15th March 2023
Accepted 26th March 2023

DOI: 10.1039/d3ra01720f

rsc.li/rsc-advances

1. Introduction

During recent decades, the design of recyclable catalysts has been greatly developed in the chemical and pharmaceutical industries.[1] Hence, anchoring catalysts to suitable solid substrates has become very important in various fields of chemical reactions.[2,3] These materials act as an interface between homogeneous and heterogeneous catalysis for reasons such as significant efficiency, physical and chemical stability, recyclability, large surface/volume ratio, and good biocompatibility.[1–5] In particular, Fe_3O_4 nanoparticles have garnered a lot of interest in organic synthesis and other fields of science due to their unique properties.[6–8] Perhaps the best feature of magnetic nanoparticles, which increases the versatility of work up steps, is their simple segregation from reaction mixtures *via* an external magnet.[6–8] In this same regard, different forms of mesoporous silica have attracted attention by reason of their unique properties in the fields of catalysis.[2,3] Among these properties, we can mention their uniform and large pore size for stabilizing metals and organic ligands, their ability to be used in harsh reaction conditions due to thermal stability above 900 °C, as well as high loading capacity to immobilize catalysts due to their high surface area (>1200 $m^2\ g^{-1}$).[9,10] These characteristics encourage chemists to place Fe_3O_4 particles in the mesoporous silica channels for the synthesis of magnetic silica nanoparticles and in this way benefit these materials as substrates for various kinds of catalysts.[9,10]

In organic and medicinal chemistry, there has been a lot of interest in multi-component reactions, sometimes known as MCRs.[11] This reactions are well-known, practical and useful protocols which have been used for production of a wide range of organic compounds.[11] MCRs that result in the production of a heterocycle core are of significant interest due to the fact that a heterocyclic scaffold is a necessary component of a great deal of pharmaceuticals and biologically active compounds.[12] They are reactions that combine three or more small-molecular-

[a]*Department of Pharmacy (Pharmaceutics), Baghdad College of Medical Sciences, Baghdad, Iraq*

[b]*Department of Chemistry, College of Science, King Saud University, P.O. Box 2455, Riyadh 11451, Saudi Arabia. E-mail: mtayyab@ksu.edu.sa; mohdubaidullah2007@gmail.com*

[c]*Department of Materials Science and Engineering and Chemical Engineering, Universidad Carlos III de Madrid, Avenida de la Universidad 30, 28911 Leganés, Madrid, Spain*

[d]*Biomedical Engineering Department, Al-Mustaqbal University College, 51001, Hillah, Iraq*

[e]*Department of General Studies, Universidad Continental, Lima, Peru*

[f]*Chief Researcher of the Institute of General and Inorganic Chemistry, Academy of Sciences of the Republic of Uzbekistan, Mirzo Ulugbek avenue 77A, 100071, Uzbekistan, Tashkent*

[g]*Department of Pharmacy, Kut University College, Kut 52001, Wasit, Iraq*

[h]*Department of Anesthesia, College of Health & Medical Technology, Al-Ayen University, Thi-Qar, Iraq*

[i]*College of Pharmacy, The Islamic University, 54001 Najaf, Iraq*

[j]*Al-Nisour University College, Baghdad, Iraq*

† Electronic supplementary information (ESI) available: The spectroscopic and physical data of pyrido-dipyrimidines. See DOI: https://doi.org/10.1039/d3ra01720f

weight building components into a single product with good selectivity and combinatorial effectivity. In addition, MCRs save time, reduce the amount of energy that is used, increase the amount of raw materials that are consumed, limit or eliminate the synthesis of waste and byproducts, and lower the amount of volatile organic solvents that are used.[12–14] In light of this, the application of this approach complies well with the protocols of green chemistry; in addition, the application of this technique is simpler and more cost-effective in comparison to traditional multi-step reactions.[12–15]

Transition metals on solid supports, and also oxides of these metals have been used as effective catalysts in various chemical reactions, including oxidation and reduction,[16–19] C–S, C–O and C–C coupling,[3,20–22] and multicomponent reactions.[3,23–25] Rapid

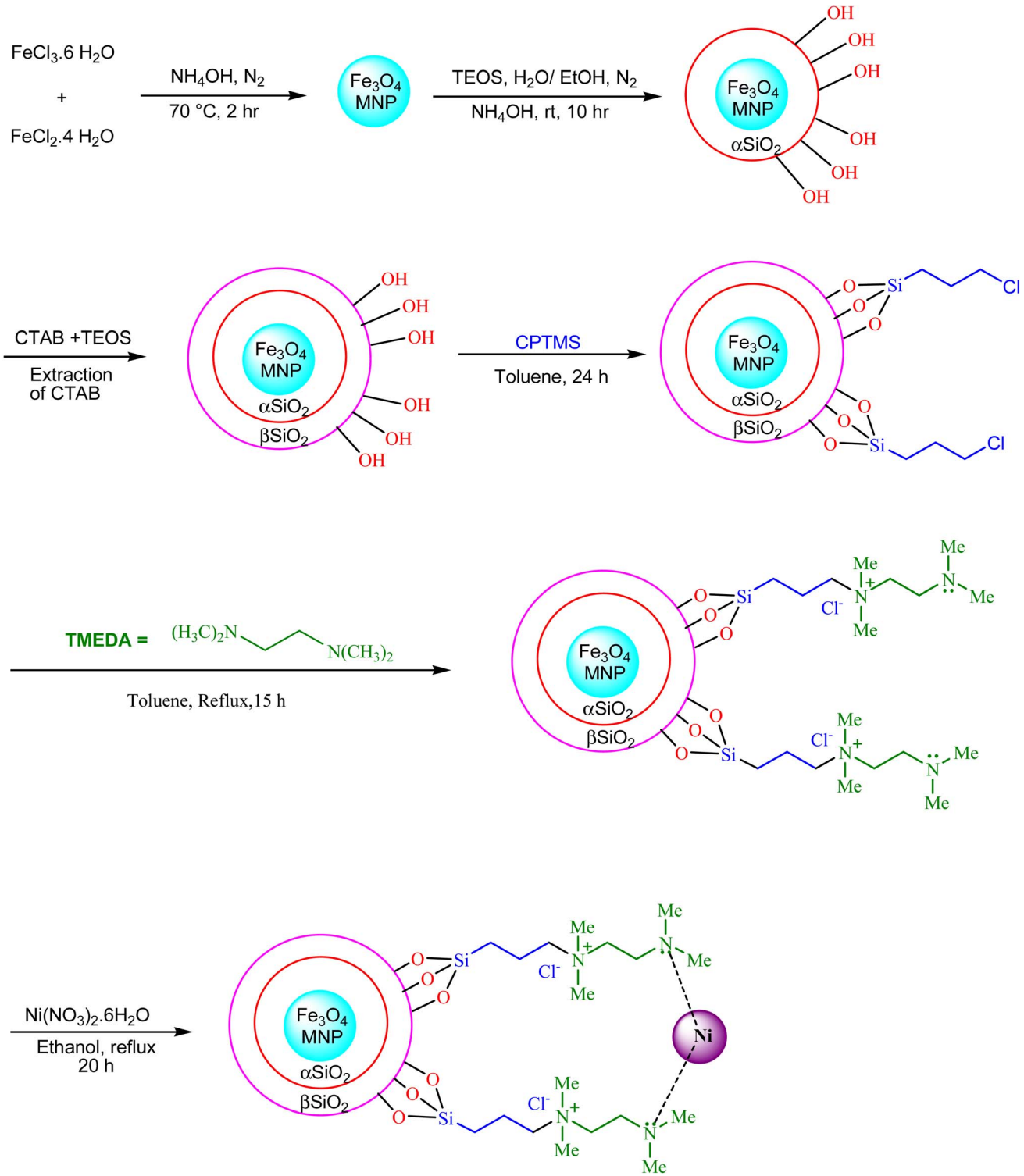

Scheme 1 Synthesis of Ni-TMEDA@βSiO_2@αSiO_2@Fe_3O_4.

development in this field is taking place due to its importance in biological, pharmaceutical, industrial and chemical fields.[25] Among transition metals, nickel is a versatile catalyst that able to use in a different of synthetic transformations.[25] In the literature, the advances in the field of nickel-catalyzed multi-component reactions are mentioned.[25]

Heterocyclic compounds containing pyrido-pyrimidine framework are of importance because they are an vital moiety of many drugs and biological active substances, such as anti-inflammatory,[26] antimicrobial,[27] antihypertensive,[28] anti-allergic,[29] anticonvulsants,[30] calcium channel antagonists, antibacterial,[31] fibroblast growth factors (FGFs),[32] anti-HIV,[33] antifolate,[34] and potassium sparing agents.[35] They have been also utilized as anticancer agents in the control of tyrosine kinases.[36,37] The one-pot MCR of arylaldehydes with 2-thio-barbituric acid and NH_4OAc has been applied as a useful synthetic route toward pyrido[2,3-*d*:6,5-*d*′]dipyrimidines; few catalysts have been reported for this synthesis.[2,38–45] Among these catalysts, we rarely come across cases where the synthesis of these compounds occurs at room temperature without the need for high temperatures or energies such as ultrasound and microwaves.[42,43] This is something that should be taken into consideration.

According to the above points, we report here Ni-TMEDA@βSiO_2@αSiO_2@Fe_3O_4 as a highly effective and magnetic nanocatalyst for the preparation of pyrido[2,3-*d*:6,5-*d*′] dipyrimidine derivatives through the Hantzsch reaction in water solvent at 25 °C under mild conditions.

2. Experimental

2.1. Preparation of Fe_3O_4

In order to prepare magnetic nanoparticles made of iron oxide (Fe_3O_4) using the chemical co-precipitation process, at first, 1.165 gr of $FeCl_3 \cdot 6H_2O$ was added to a solution that included 100 mL of H_2O and 0.429 g of $FeCl_2 \cdot 4H_2O$. The mixture was stirred for two hours at 70 °C under N_2 atmosphere. After that, 20 mL of ammonia was added to the combination of reactants in a drop-by-drop fashion. After a total of three hours of stirring, the finished mixture was cooled to room temperature. By means of an outside magnet, the black precipitate was separated and rinsed in hot, deionized water six times. The resulting nano-Fe_3O_4 was then dried for 8 hours at 80 °C (Scheme 1).[46]

2.2. Preparation of βSiO_2@αSiO_2@Fe_3O_4

In order to create silica-coated magnetite, 2.5 g of Fe_3O_4 nanoparticles were diluted with 160 mL of deionized H_2O and 300 mL of ethanol, and then this solution was dispersed in an ultrasonic bath for a period of forty minutes. The combination was then given an addition of 5 mL of a concentrated ammonia aqueous solution. This step took place in the presence of N_2. After that, 2 mL of tetraethyl orthosilicate were gradually added to this dispersion while stirring it at a temperature of 25 °C for ten hours. Finally, the αSiO_2@Fe_3O_4 nanoparticles were separated employing a magnet, washed many times in EtOH and distilled H_2O, and dried at 60 °C. Nanoporous SiO_2 shells were covered on the particles *via* dispersing the produced αSiO_2@-Fe_3O_4 (0.1 g) in a solution including cetyltrimethyl ammonium bromide (CTAB, 0.3 g), EtOH (40 mL), NH_4OH (25 wt%, 1 mL) and distilled H_2O (60 mL). In continue 0.5 mL TEOS were added (drop by drop) into the suspension, then the solution produced was stirred for 20 h (at 25 °C). In the next step, the βSiO_2@-αSiO_2@Fe_3O_4 was isolated by external magnet and washed and dried using the procedure expressed in the previous section (Scheme 1).

2.3. Preparation of Ni-TMEDA@βSiO_2@αSiO_2@Fe_3O_4

At this stage, to prepare nPr-Cl@βSiO_2@αSiO_2@Fe_3O_4, first 2 g of βSiO_2@αSiO_2@Fe_3O_4 were sonicated in 60 mL of *n*-hexane for 35 min, after that, 3.5 milliliters 3-chloropropyltrimethoxysilane (CPTMS) was added to the solution that had been prepared and stirred for 24 hours in toluene reflux. Then, magnetic nanoparticles (nPr-Cl @βSiO_2@αSiO_2@Fe_3O_4) were washed with ethanol, separated with an external magnet, and dried at 50 °C. Next, the nPr-Cl @βSiO_2@αSiO_2@Fe_3O_4 MNPs solid (1 g) is mixed with (1 mmol) *N*,*N*,*N*′,*N*′-tetramethylethane-1,2-diamine in toluene (15 mL) and let to stand at 115 °C for 15 hours to immobilize the TMEDA on the surface of the MNPs. In the last step of the method, nickel was immobilized onto TMEDA@βSiO_2@αSiO_2@Fe_3O_4. This was accomplished by first dissolving 1 gr of TMEDA@βSiO_2@αSiO_2@Fe_3O_4 NPs in ethanol, and then adding $Ni(NO_3)_2 \cdot 6H_2O$ (4 mmol, 1.163 g) to the resulting mixture. The resultant mixture was subjected to a total of twenty hours of agitation while in a condition of reflux. The Ni-TMEDA@βSiO_2@αSiO_2@Fe_3O_4 NPs that had been generated were eventually dried in an air environment after being filtered and washed with ethanol many times (Scheme 1).

2.4. General method for the preparation of pyrido[2,3-*d*:6,5-*d*′]dipyrimidines using a by catalyst Ni-TMEDA@βSiO_2@αSiO_2@Fe_3O_4

A mixture that included 2-thiobarbituric acid (2 mmol, 0.288 g), NH_4OAc (1.3 mmol 0.100 g), aldehyde (1 mmol), Ni-TMEDA@βSiO_2@αSiO_2@Fe_3O_4 (2.6 mol%, 0.01 g), and H_2O (2 mL) as a solvent was agitated at a temperature of 25 °C. After

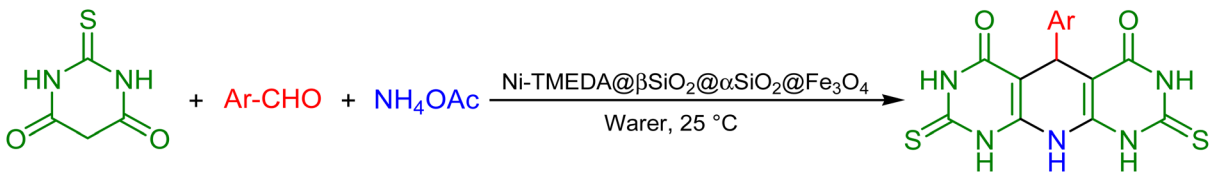

Scheme 2 Ni-TMEDA@βSiO_2@αSiO_2@Fe_3O_4 catalyzed the synthesis pyrido[2,3-*d*:6,5-*d*′]dipyrimidines.

completion of the reaction (as observed by TLC), 20 mL of H_2O was added to the reaction mixture, stirred for 1 min (at 50 °C), and filtered to separate the catalyst (in the presence of a magnet). The isolated catalyst was washed by EtOH (2 × 3 mL), dried and used for next run. Finally, the water was evaporated, and the remainder precipitate was recrystallized from EtOH (96%) to afford the pure product (Scheme 2).

3. Results and discussion

3.1. Catalyst characterization

FT-IR data of Fe_3O_4, $\beta SiO_2@\alpha SiO_2@Fe_3O_4$, TMEDA@$\beta SiO_2@\alpha SiO_2@Fe_3O_4$ and Ni-TMEDA@$\beta SiO_2@\alpha SiO_2@Fe_3O_4$ are summarized in Table 1 (Fig. 1). These data confirm the presence of the expected bonds, the immobilization of SiO_2 on Fe_3O_4 and the subsequent formation of TMEDA@$\beta SiO_2@\alpha SiO_2@Fe_3O_4$. Also, the functionalization of $\beta SiO_2@\alpha SiO_2@Fe_3O_4$ with TMEDA was exhibits by stretching vibration of C–N at 1386 cm^{-1}, which this band was shifted to lower frequency in the Ni-TMEDA@$\beta SiO_2@\alpha SiO_2@Fe_3O_4$ (1382 cm^{-1}), which is due to the coordination of Ni to supported TMEDA onto functionalized $\beta SiO_2@\alpha SiO_2@Fe_3O_4$.[47] Based on these observations, the well anchoring of nickel onto TMEDA@$\beta SiO_2@\alpha SiO_2@Fe_3O_4$ is verified.

The scanning electron microscope (SEM) method was used in order to produce high-resolution pictures of Ni-TMEDA@$\beta SiO_2@\alpha SiO_2@Fe_3O_4$. The images obtained from this technique were employed to specify the morphology of the catalyst; these images show that most of the particles are quasi-spherical (Fig. 2(a)). Also, the particle size distribution of the Ni-TMEDA@$\beta SiO_2@\alpha SiO_2@Fe_3O_4$ demonstrated that these nanoparticles have a size in the range of 10–100 nm and an average diameter of 47.72 nm (Fig. 2(b)).

The TEM micrograph of Ni-TMEDA@$\beta SiO_2@\alpha SiO_2@Fe_3O_4$ is shown in Fig. 3; we observe quasi-spherical cases from the micrograph. The calculated amount of Ni in nanocatalyst which was achieved *via* inductively coupled plasma (ICP) analysis was found to be 2.6×10^{-3} mol g^{-1}.

EDX analysis of the Ni-TMEDA@$\beta SiO_2@\alpha SiO_2@Fe_3O_4$ was carried out so that the elements that were present in the catalyst structure could be identified (Fig. 4). This study reveals the presence of carbon, oxygen, silicon, nitrogen, iron, and nickel. In addition to this, the outcomes of the EDS were validated by the elemental mapping analysis, as demonstrated in (Fig. 5).

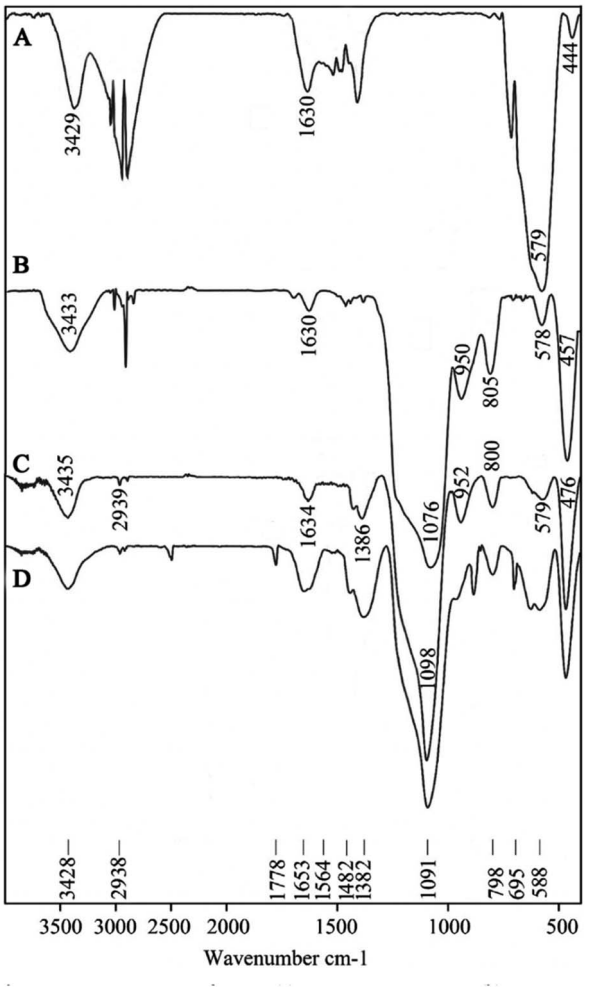

Fig. 1 The FT-IR spectrums of Fe_3O_4 (A), $\beta SiO_2@\alpha SiO_2@Fe_3O_4$ (B), TMEDA@$\beta SiO_2@\alpha SiO_2@Fe_3O_4$ (C) and Ni-TMEDA@$\beta SiO_2@\alpha SiO_2@Fe_3O_4$ (D).

Homogeneous distribution of all elements and dispersion of nickel throughout the support was clearly observed in this analysis.

The VSM technique was used to evaluate the magnetic properties of Fe_3O_4 and Ni-TMEDA@$\beta SiO_2@\alpha SiO_2@Fe_3O_4$. As can be seen in Fig. 6, Ni-TMEDA@$\beta SiO_2@\alpha SiO_2@Fe_3O_4$ has a lower magnetic value than Fe_3O_4. This is because organic

Table 1 The FT-IR data of Fe_3O_4 (A), $\beta SiO_2@\alpha SiO_2@Fe_3O_4$ (B), TMEDA@$\beta SiO_2@\alpha SiO_2@Fe_3O_4$ (C) and Ni-TMEDA@$\beta SiO_2@\alpha SiO_2@Fe_3O_4$ (D)

Peak (spectrum name) (cm^{-1})	Assignments
579 (A), 578 (B), 579 (C), 588 (D)	Fe–O stretching[47]
805 (B), 800 (C), 798 (D)	Si–O–Si symmetric stretching[2]
950 (B), 952 (C), ~950 (D)	Si–O–Fe stretching[2]
1076 (B), 1098 (C), 1091 (D)	Si–O–Si asymmetric stretching[47]
1386 (C), 1382 (D)	C–N stretching[2]
~1482 (C), 1482 (D)	CH_2 bending[2]
1630 (A), 1630 (B), 1634 (C), 1653 (D)	OH bending on the surface of the Fe_3O_4 and SiO_2 (ref. 2 and 47)
2939 (C), 2938 (D)	C–H symmetric stretching[2]
3429 (A), 3433 (B), 3435 (C), 3428 (D)	OH stretching on the surface of the Fe_3O_4 and SiO_2 (ref. 2 and 47)

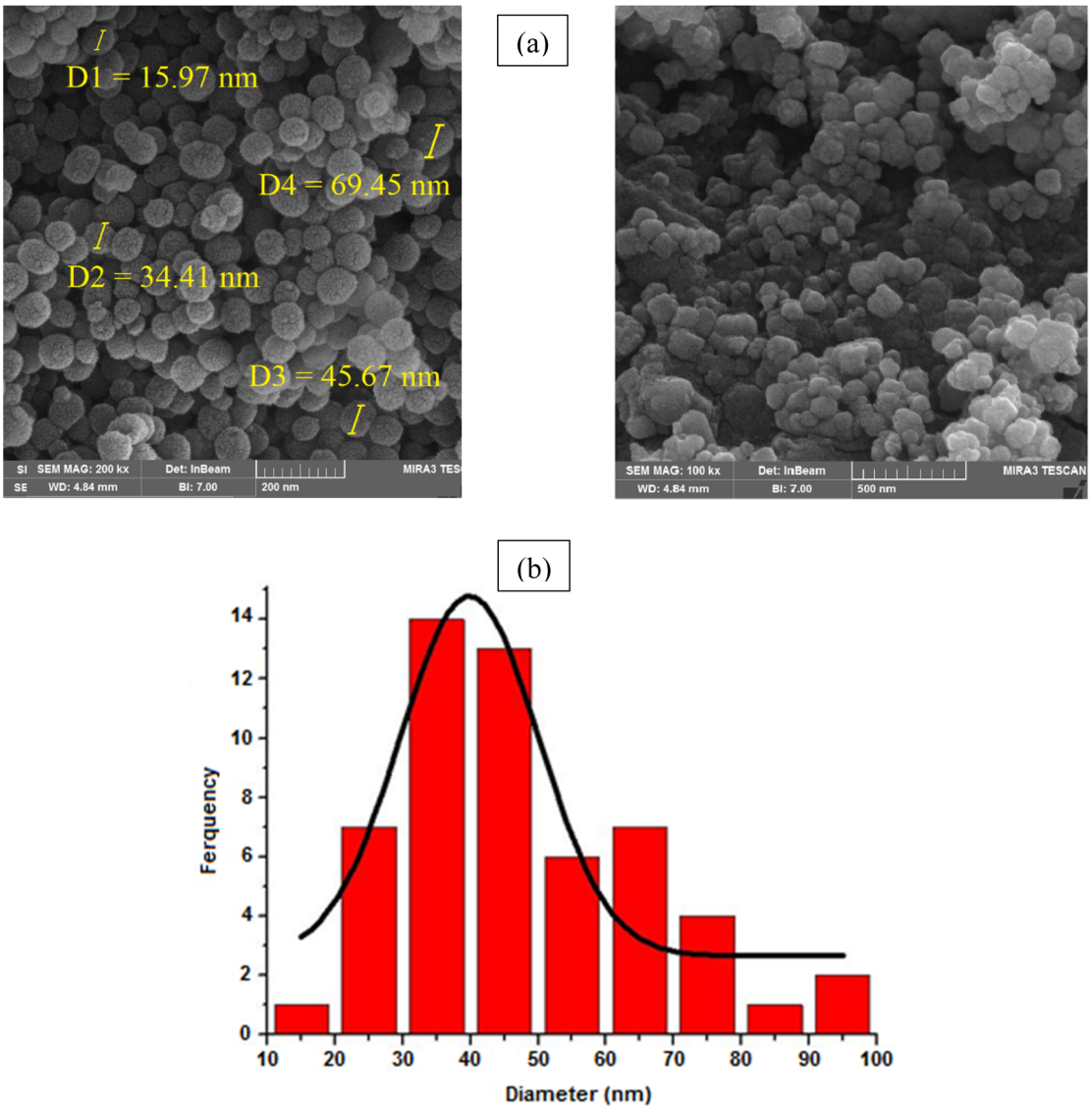

Fig. 2 The FE-SEM images (a) and particle size distribution (b) of Ni-TMEDA@βSiO$_2$@αSiO$_2$@Fe$_3$O$_4$.

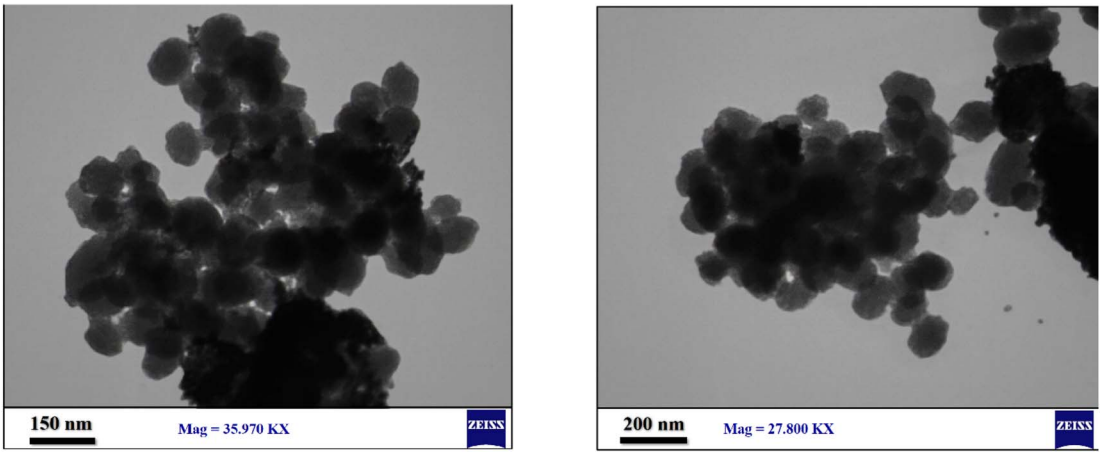

Fig. 3 The TEM Ni-TMEDA@βSiO$_2$@αSiO$_2$@Fe$_3$O$_4$.

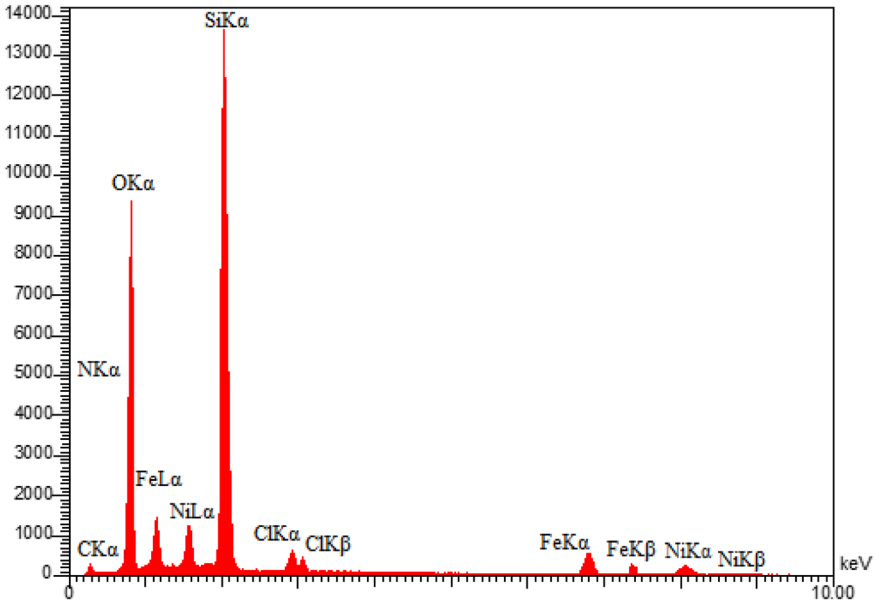

Fig. 4 The EDX Ni-TMEDA@βSiO$_2$@αSiO$_2$@Fe$_3$O$_4$.

groups act as a shield for the surface of Fe$_3$O$_4$, reducing its magnetic strength.

The XRD spectrum of Ni-TMEDA@βSiO$_2$@αSiO$_2$@Fe$_3$O$_4$ was studied at $2\theta = 10°$ to 80° (Fig. 7); in this spectrum, the diffraction lines observed at $2\theta = 33.4°$, 38.3°, 42.7°, 54.4°, 58.4° and 61.7° are related to the crystalline nature of Fe$_3$O$_4$ particles.[47] These findings affirmed that the modification of SiO$_2$ nanoparticles on Fe$_3$O$_4$ did not lead to a changes in the crystalline nature of magnetite nanoparticles; this is in accordance with the previous literature.[48] The Bragg angles (2θ) at 44.5 (111), 50.6 (200) and 73.4 (220) confirmed the presence of nickel in the catalyst and its immobilization on βSiO$_2$@αSiO$_2$@Fe$_3$O$_4$.[49] Also, the broad peak observed at 2θ = 20°-30° is associated to the silica skeleton (especially amorphous silica) in the catalyst body;[2] the amorphous and crystalline percentages of Ni-TMEDA@βSiO$_2$@αSiO$_2$@Fe$_3$O$_4$ were 21.56 and 78.44%, respectively.

The thermal stability diagram of Ni-TMEDA@βSiO$_2$@αSiO$_2$@Fe$_3$O$_4$ is displayed in Fig. 8. In the first stage, the TGA diagram demonstrates a weight loss of 6% at temperatures below 200 °C, which is possibly associated with the elimination of adsorbed organic solvents.[3,48] The weight loss of the second stage (~7%) in this graph, which occurs in the temperature range of 250–700 °C, can be related to the decomposition of immobilized organic groups on the surface of Fe$_3$O$_4$. These data provide compelling evidence that the material has a high thermal stability.[3,48]

Nitrogen adsorption desorption method was used to investigate the porosity of Ni-TMEDA@βSiO$_2$@αSiO$_2$@Fe$_3$O$_4$ nanocatalyst and its producing components (Fig. 9–11). The results of this study are summarized in Table 2. Based on the data in this table, the specific surface area of Ni-TMEDA@βSiO$_2$@αSiO$_2$@Fe$_3$O$_4$ has decreased compared to TMEDA@βSiO$_2$@αSiO$_2$@Fe$_3$O$_4$, αSiO$_2$@Fe$_3$O$_4$ and Fe$_3$O$_4$; this is due to the stabilization of organic groups and nickel complexes on the mesoporous channels of magnetic silica nanoparticles.[50,51] The specific surface (S_{BET}) of each material can be calculated through eqn (1), where, A_{N_2} is atomic surface area of N_2 at 77 K (0.162 nm^2), N and V_m are the Avogadro's number and monolayer volume, respectively (eqn (2)).[52]

$$S_{BET} = \frac{0.001 \times V_m}{22.4} \times N \times A_{N_2} \quad (1)$$

$$S_{BET} = \frac{0.001 \times 75.815\ \text{cm}^3\ \text{g}^{-1}}{22.4\ \text{cm}^3\ \text{mol}^{-1}} \times 6.022 \times 10^{23}\ \text{mol}^{-1} \times 0.162 \times 10^{-18}\ \text{m}^2 = 330.18\ \text{m}^2\ \text{g}^{-1} \quad (2)$$

3.2. Study of catalytic property

After successful synthesis and characterization of Ni-TMEDA@βSiO$_2$@αSiO$_2$@Fe$_3$O$_4$ catalyst, its catalytic performance was carefully investigated in the preparation of pyrido[2,3-*d*:6,5-*d*′]dipyrimidines at room temperature. In this regard, for selection of the best catalyst amount, type and amount of solvent, the condensation of 2-nitrobenzaldehyde (1 mmol) with 2-thiobarbituric acid (2 mmol) and NH$_4$OAc (1.3 mmol) was chosen as a model reaction (Scheme 1), and examined in the presence of different amounts of Ni-TMEDA@βSiO$_2$@αSiO$_2$@Fe$_3$O$_4$ using various solvents. The results are briefed in Table 3. As it is indicated in this Table, higher yield of the product was acquired in shorter time by utilization of 0.01 g of nanomagnetic catalyst in water solvent (2 mL) (Table 3, entry 2). The reason for this is that non-polar solvents are unsuitable for dissolving ammonium acetate salt (Table 3, entries 6–8); also, the results showed that the mixture of water and ethanol (3 : 1) was equally effective but in a longer time (Table 3, entry 9). In

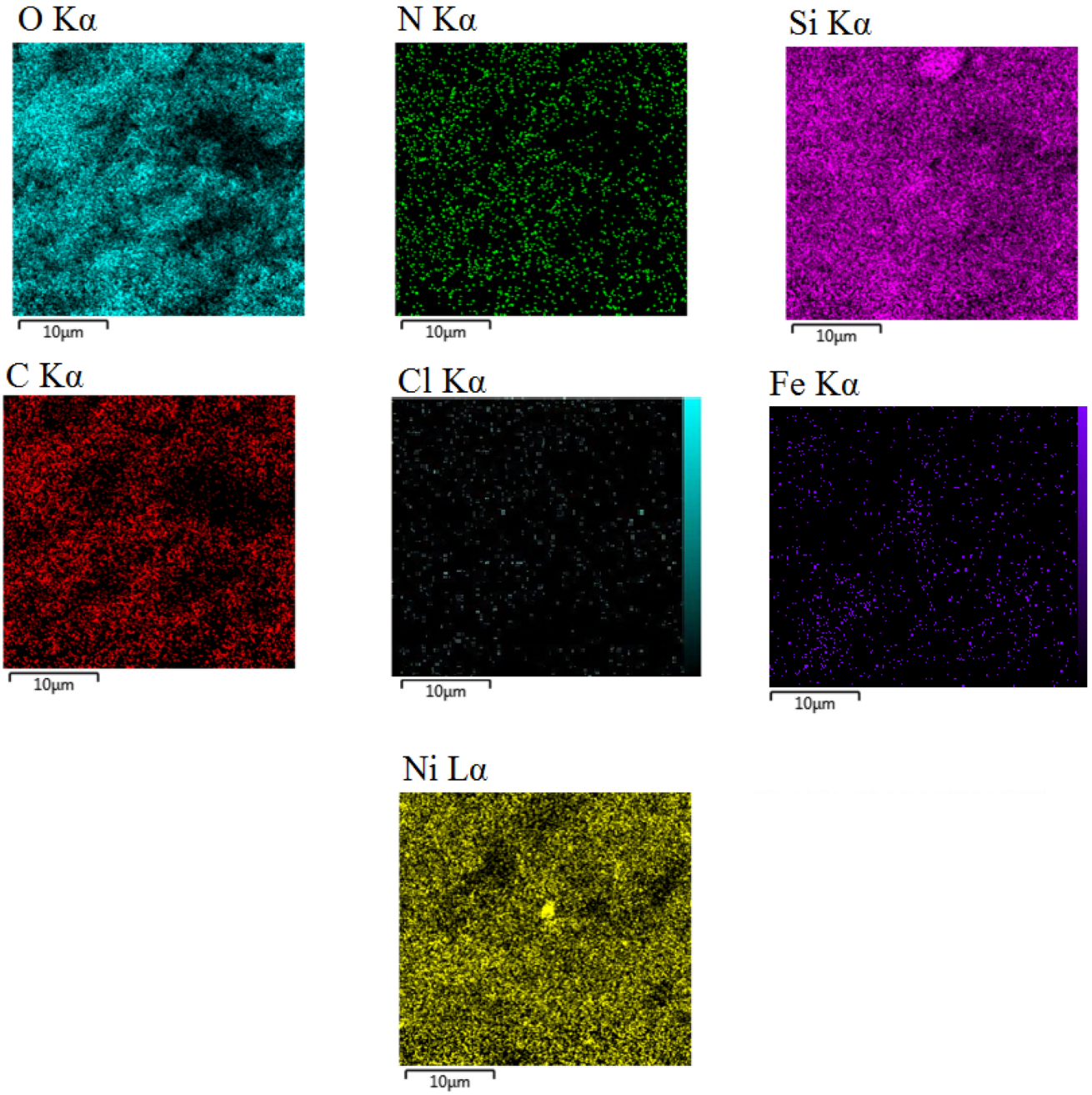

Fig. 5 The mapping of Ni-TMEDA@βSiO$_2$@αSiO$_2$@Fe$_3$O$_4$.

another research, the reaction was examined under optimal conditions in the presence of the reactants for the synthesis of Ni-TMEDA@βSiO$_2$@αSiO$_2$@Fe$_3$O$_4$, *i.e.* TMEDA (Table 3, entry 10), Fe$_3$O$_4$ (Table 3, entry 11), βSiO$_2$@αSiO$_2$@Fe$_3$O$_4$ (Table 3, entry 12), TMEDA@βSiO$_2$@αSiO$_2$@Fe$_3$O$_4$ (Table 3, entry 13), and also Ni(NO$_3$)$_2$·6H$_2$O (Table 3, entry 14), and Ni-TMEDA@αSiO$_2$@Fe$_3$O$_4$ (which prepared using monolayer of silica) (Table 3, entry 15). Then, the amount of nickel in the Ni-TMEDA@βSiO$_2$@αSiO$_2$@Fe$_3$O$_4$ and Ni-TMEDA@αSiO$_2$@ Fe$_3$O$_4$ was calculated through Inductively Coupled Plasma (ICP) analysis, which was equal to 2.6×10^{-3} and 1.4×10^{-3} mol g^{-1}, respectively. The results from Table 3 and ICP analysis showed that our strategy of using two layers of silica (αSiO$_2$ and βSiO$_2$) on Fe$_3$O$_4$ and also immobilizing nickel on the TMEDA@βSiO$_2$@αSiO$_2$@Fe$_3$O$_4$ was useful to promote the reaction efficiently, because none of the components of the catalyst alone have a significant role in the progress of the reaction, but when they are connected to each other and form the catalyst, they show a strong synergistic effect. Using two layers of silica on Fe$_3$O$_4$ causes more organic groups and thus more nickel metal to enter the mesoporous channels. In addition, the immobilization of SiO$_2$ on Fe$_3$O$_4$ prevents the aggregation of Fe$_3$O$_4$ particles (Scheme 3).

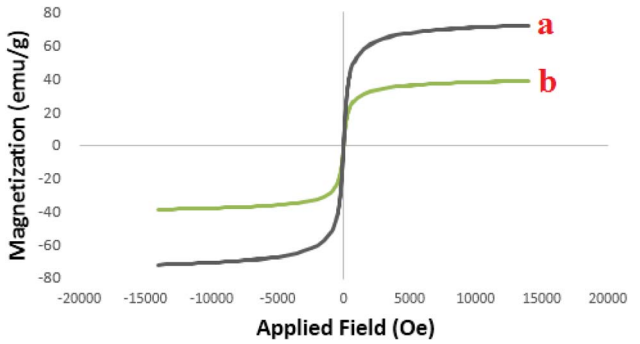

Fig. 6 Magnetization curves for Fe_3O_4 (a) and Ni-TMEDA@βSiO_2@αSiO_2@Fe_3O_4 (b).

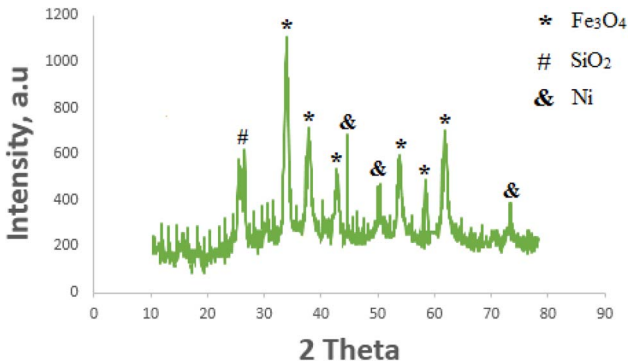

Fig. 7 The XRD pattern of Ni-TMEDA@βSiO_2@αSiO_2@Fe_3O_4.

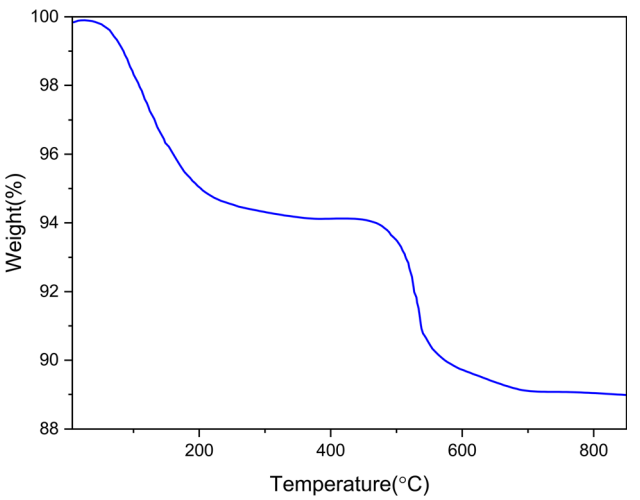

Fig. 8 TGA analysis of Ni-TMEDA@βSiO_2@αSiO_2@Fe_3O_4.

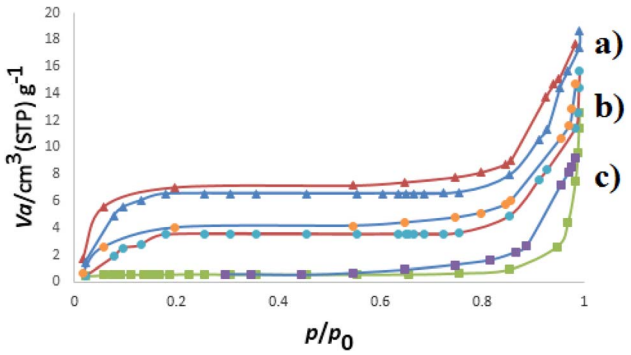

Fig. 9 Nitrogen adsorption–desorption isotherms of (a) αSiO_2@Fe_3O_4 (b) TMEDA@βSiO_2@αSiO_2@Fe_3O_4 (c) Ni-TMEDA@βSiO_2@αSiO_2@Fe_3O_4.

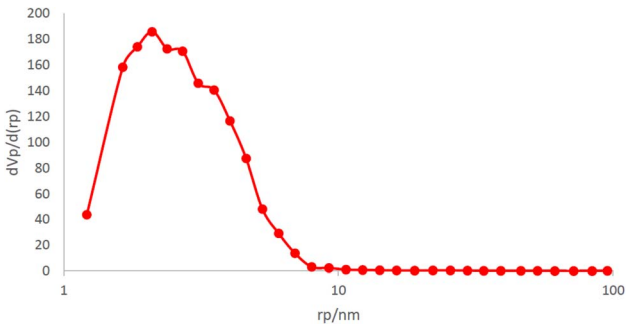

Fig. 10 The pore size distribution (BJH model) of Ni-TMEDA@βSiO_2@αSiO_2@Fe_3O_4.

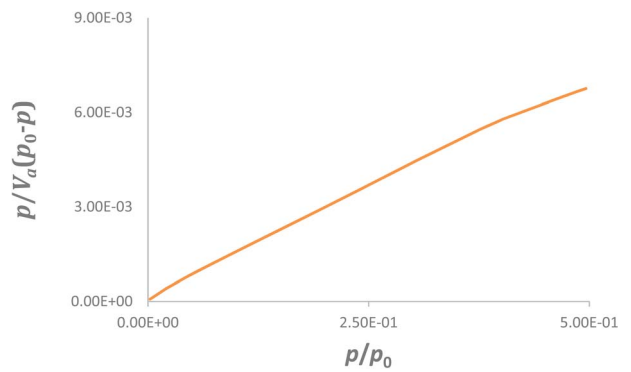

Fig. 11 The BET curve of Ni-TMEDA@βSiO_2@αSiO_2@Fe_3O_4.

To confirm that Ni-TMEDA@βSiO_2@αSiO_2@Fe_3O_4 is general and effectual catalyst for the synthesis of pyrido-dipyrimidines, various aromatic aldehydes were reacted with 2-thiobarbituric acid and NH_4OAc under the optimal conditions. In this investigation, arylaldehydes bearing electron-attracting, halogens and electron-donating substituents on *ortho*, *meta* and *para* positions were exerted. The results are displayed in Table 4. As the data in this table illustrate, arylaldehydes bearing halogen, electron-releasing and electron-withdrawing substituents on *ortho*, *meta* and *para* positions afforded the relevant products in high yields and short times as well as high TON and TOF values. Accordingly, Ni-TMEDA@βSiO_2@αSiO_2@Fe_3O_4 was general and highly effectual catalyst for the reaction at room temperature.

A performance of Ni-TMEDA@βSiO_2@αSiO_2@Fe_3O_4 for the production of pyrido-dipyrimidines in comparison with previous literature in this field by comparing factors such as TOF, TON, yield, time and the reaction temperature in the

Table 2 Texture properties of Ni-TMEDA@αSiO$_2$@βSiO$_2$@Fe$_3$O$_4$

Sample	SBET (m^2 g^{-1})	Pore diam by BJH method (nm)	Pore vol (cm^3 g^{-1})	Ref.
Fe_3O_4	480.0	1.254	0.803	50
$\alpha SiO_2@Fe_3O_4$	455.2	1.564	0.789	—
TMEDA@$\beta SiO_2@\alpha SiO_2@Fe_3O_4$	404.6	1.798	0.716	—
Ni-TMEDA@$\beta SiO_2@\alpha SiO_2@Fe_3O_4$	330.1	2.012	0.621	—

Table 3 Investigating influence of catalyst, catalyst amount, type and amount of solvent on the model reaction

Entry	Catalyst	Catalyst amount (g)	Solvents	Solvent amount (mL)	Time (min)	Yield[a] (%)
1	Ni-TMEDA@$\beta SiO_2@\alpha SiO_2@Fe_3O_4$	0.01	H_2O	2	25	80
2	Ni-TMEDA@$\beta SiO_2@\alpha SiO_2@Fe_3O_4$	0.02	H_2O	2	15	99
3	Ni-TMEDA@$\beta SiO_2@\alpha SiO_2@Fe_3O_4$	0.03	H_2O	2	15	99
4	Ni-TMEDA@$\beta SiO_2@\alpha SiO_2@Fe_3O_4$	0.02	H_2O	1	15	90
5	Ni-TMEDA@$\beta SiO_2@\alpha SiO_2@Fe_3O_4$	0.02	H_2O	3	20	99
6	Ni-TMEDA@$\beta SiO_2@\alpha SiO_2@Fe_3O_4$	0.02	EtOH	2	15	76
7	Ni-TMEDA@$\beta SiO_2@\alpha SiO_2@Fe_3O_4$	0.02	Acetone	2	30	39
8	Ni-TMEDA@$\beta SiO_2@\alpha SiO_2@Fe_3O_4$	0.02	CH_3CN	2	30	42
9	Ni-TMEDA@$\beta SiO_2@\alpha SiO_2@Fe_3O_4$	0.02	H_2O/EtOH (3 : 1)	2	20	99
10	TMEDA	0.02	H_2O	2	15	Trace
11	Fe_3O_4	0.02	H_2O	2	15	32
12	$\beta SiO_2@\alpha SiO_2@Fe_3O_4$	0.02	H_2O	2	15	35
13	TMEDA@$\beta SiO_2@\alpha SiO_2@Fe_3O_4$	0.02	H_2O	2	15	40
14	$Ni(NO_3)_2 \cdot 6H_2O$	0.02	H_2O	2	15	Trace
15	Ni-TMEDA@$\alpha SiO_2@Fe_3O_4$	0.02	H_2O	2	15	70

[a] Yield of isolated product.

preparation of pyrido[2,3-*d*:6,5*d*′]dipyrimidine derivatives in the Table 5 have been reported. According to the data in the table, our c catalyst had a significant advantage over other catalysts in at least three or four comparative factors.

Based on the previous literature, which used supported nickel as an electrophilic activator,[3,23] a logical mechanism for the synthesis of pyrido-dipyrimidine derivatives using our catalyst is presented in Scheme 4.[38–40] Initially, the activated aldehyde by nickel as the active center of nanocatalyst reacts with intermediate II (which is produced as a result of the activation of tautomer I of 2-thiobarbituric acid in the presence of a catalyst) to provide intermediate III after removal of a water molecule. In the other hand, the activated another molecule of tautomer I by catalyst reacts with ammonia to form intermediate IV after removal of a H_2O molecule. The next step is a michael addition of intermediate IV to intermediate III (which activated with catalyst), and tautomerization to form intermediate V. Finally, pyrido-dipyrimidine is produced by the intermolecular nucleophilic attack of the amine nitrogen to its activated carbonyl group in intermediate V, and elimination of a H_2O molecule.

3.3. Reusability of the nanocatalyst

In both the laboratory and the industrial settings, the fact that the catalysts may be recycled several times is an essential consideration. Therefore, the reusability of Ni-TMEDA@$\beta SiO_2@\alpha SiO_2@Fe_3O_4$ was investigated during the synthesis of compound **2a**; the findings obtained are summarized in Fig. 12. Recycling the catalyst was obtained by the stated method in the experimental section. The recycled catalyst was reused up to seven times without a noticeable decrease in catalytic activity. The average yields is 96.42% for 7 consecutive runs, which shows the excellent recyclability of our catalyst.

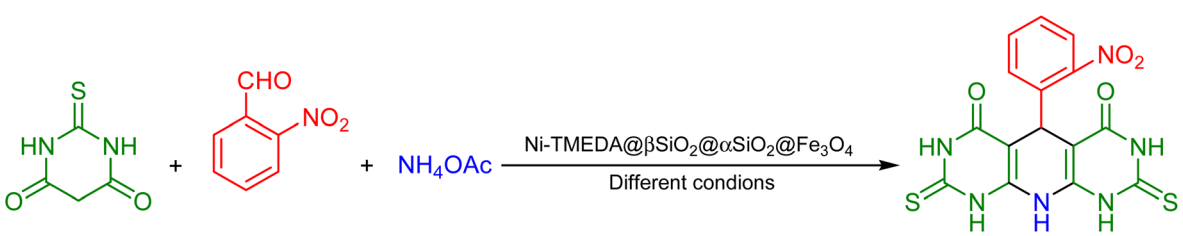

Scheme 3 The model reaction.

Table 4 The synthesis of pyrido[2,3-*d*:6,5-*d*′]dipyrimidines by Ni-TMEDA@βSiO$_2$@αSiO$_2$@Fe$_3$O$_4$[a,b]

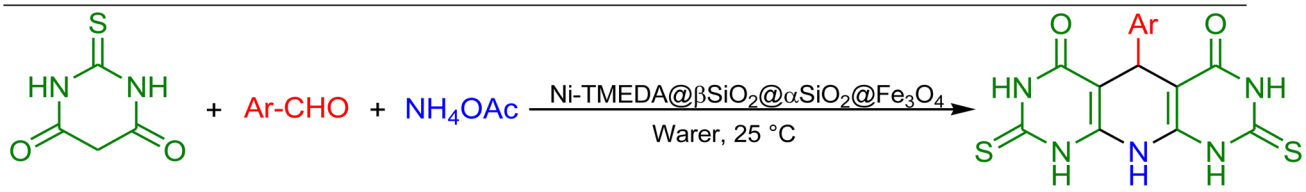

1a–16a[a]: time (min), yield (%)[b], TON, TOF (min^{-1}), ref.

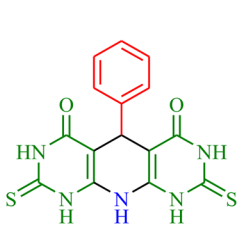

1a: 20, 98%, 37.7, 1.88, [38]

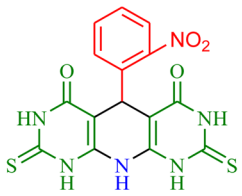

2a: 15, 99%, 38.0, 2.53, [38]

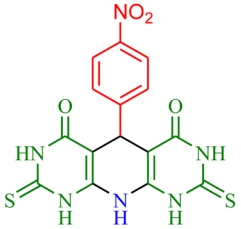

3a: 15, 98%, 37.7, 2.51, [38]

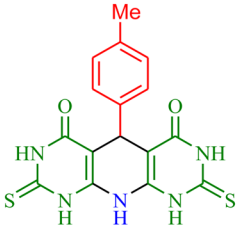

4a: 25, 91%, 35.0, 1.40, [38]

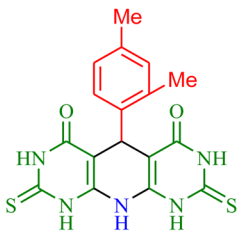

5a: 25, 90%, 34.6, 1.38

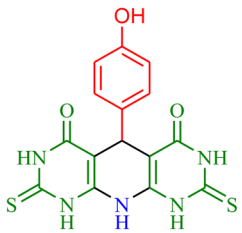

6a: 25, 91%, 35.0, 1.40

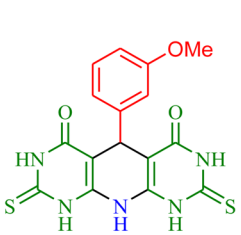

7a: 25, 90%, 34.6, 1.38, [38]

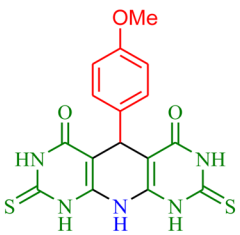

8a: 25, 95%, 36.5, 1.46, [38]

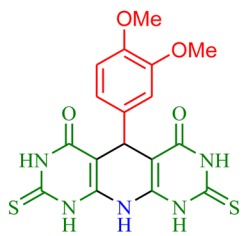

9a: 25, 92%, 35.3, 1.41, [38]

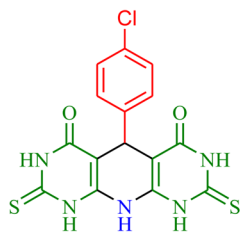

10a: 20, 96%, 36.9, 1.84, [38]

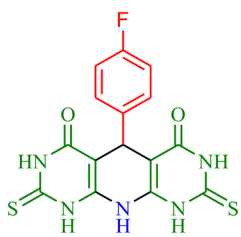

11a: 15, 96%, 36.9, 2.46, [38]

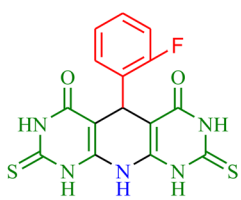

12a:15, 97%, 37.3, 2.48, [38]

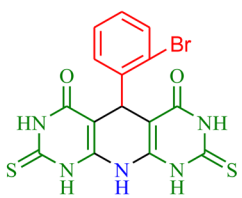

13a: 25, 97%, 37.3, 1.49, [38]

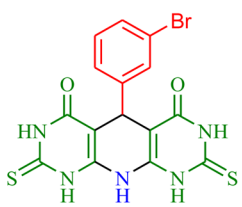

14a: 25, 98%, 37.7, 1.50, [38]

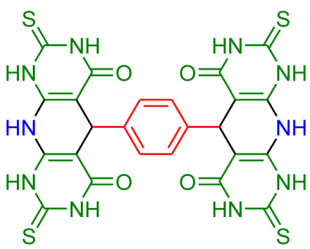

15a: 30, 94%, 36.1,1.20, [39]

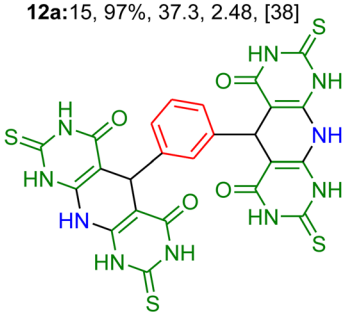

16a:30, 89%, 34.2, 1.14

[a] Reaction conditions **1a–14a:** aromatic aldehyde (1 mmol), 2-thiobarbituric acid (2 mmol), NH$_4$OAc (1.3 mmol), and catalyst (0.01 g). Also reaction conditions **15a** and **16a:** terephthalaldehyde or isophthalaldehyde (1 mmol), 2-thiobarbituric acid (4 mmol), NH$_4$OAc (2.6 mmol), and catalyst (0.01 g). [b] Isolated yield.

Table 5 Comparison of the reaction results of Ni-TMEDA@βSiO$_2$@αSiO$_2$@Fe$_3$O$_4$ with previously published catalysts in the preparation of pyrido[2,3-*d*:6,5-*d*′]dipyrimidine derivatives

Catalyst	Conditions	Time (min)	Yield (%)[a]	TON	TOF (min^{-1})	Ref.
Our catalyst	H_2O, r.t.	15–30	89–99	34.2–38.0	1.14–2.53	—
Nano-[DMSPDE][Cl][a]	Solvent-free, 110 °C	5–20	84–91	—	—	2
Nano-[SiO$_2$-R-NMe$_2$SO$_3$H][Cl]	Solvent-free, 90 °C	5–15	88–95	33.3–35.9	2.22–7.18	38
Nano $CuFe_2O_4$	H_2O, ultrasonic (40 W)	4–30	0–99	0.0–9.9	0.00–2.45	39
Nano $CuFe_2O_4$	H_2O, microwave (100 W)	1–2	90–98	9.0–9.8	4.50–9.80	40
γ-Fe$_2$O$_3$@HAp-SO$_3$H	DMF, 110 °C	20–75	70–95	7.7–10.5	0.10–0.47	41
Fe-MCM-41-IL	H_2O, r.t.	57–25	95–80	18.2–21.6	0.33–0.86	42
Nano $CuFe_2O_4$	H_2O, r.t.	120–20	99–0	0.0–9.9	0.00–0.49	43
$[HNMP]^+[HSO_4]^-$	H_2O, ultrasonic (26.5 W)	5–30	<98–5	<0.3–6.5	<0.01–1.30	44
$[Et_3N–SO_3H][MeSO_3]$	EtOH, reflux	2–5	99–93	9.3–9.9	1.86–4.95	45

[a] In this manuscript, we were unable to measure TON and TOF because the molar percentage of catalyst was not reported.

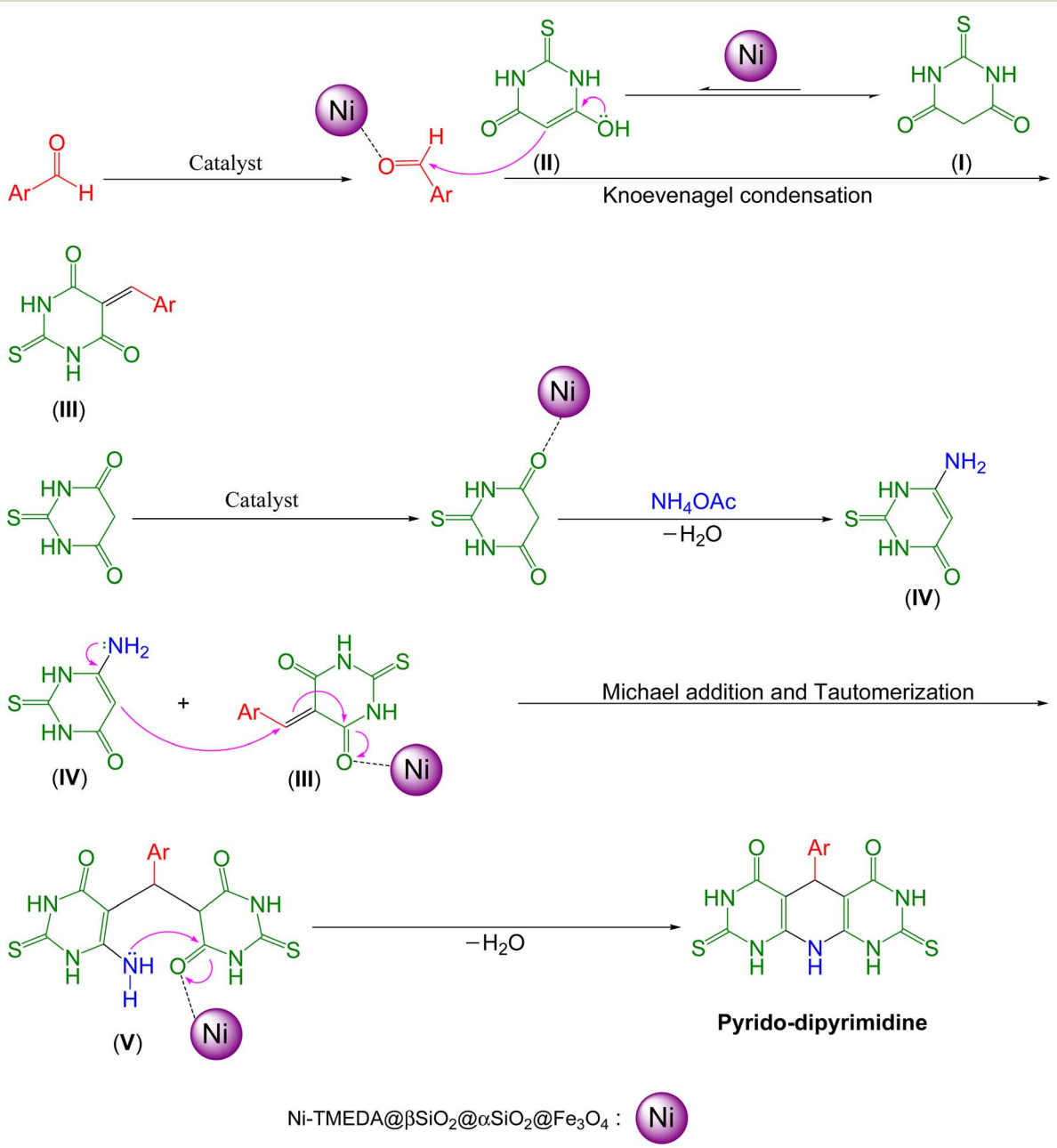

Scheme 4 The suggested mechanism for the production of pyrido-dipyrimidines.

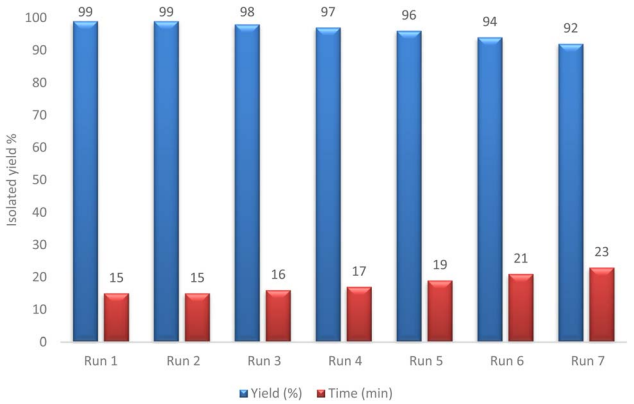

Fig. 12 The recycling experiment of Ni-TMEDA@βSiO$_2$@αSiO$_2$@Fe$_3$O$_4$ in the production of compound **2a**.

3.4. Leaching study of catalyst

For the leaching of nickel from Ni-TMEDA@βSiO$_2$@αSiO$_2$@Fe$_3$O$_4$, ICP analysis and hot filtration test was used. According to ICP analysis, the amount of Ni in the fresh and reused catalyst was 2.60 $\times$ 10^{-3} mol g^{-1} and 2.575 $\times$ 10^{-3} mol g^{-1}, respectively, which showed that Ni leaching of this catalyst is insignificant. Also, to confirm that the catalyst used is heterogeneous nature in the reaction conditions, a hot filtration test was studied for the preparation of compound **2a**. In this experiment, 53% of the product was formed in half the reaction time (reaction time 15 min). Next, this reaction was reiterated and after 7.5 min from the start of the reaction, the catalyst was detached and the filtrated solution was allowed to progress for another 7.5 min without the catalyst. After this time, only 56% of product **2a** was formed. This observation confirms that the leaching of Ni did not happen.

4. Conclusions

Concisely, an effectual and reusable heterogeneous catalyst known as Ni-TMEDA@βSiO$_2$@αSiO$_2$@Fe$_3$O$_4$ was produced and successfully used in the production of pyrido[2,3-*d*:6,5-*d*′] dipyrimidines. The current protocol provides very suitable turnover frequency (TOF) and turnover number (TON) values in the synthesis of all derivatives. This nanocatalyst has the advantages of both Fe$_3$O$_4$ (*e.g.* simple separation through an external magnet) and mesoporous silica (*e.g.* large surface area and suitable pore size for stabilizing organic ligands) systems. In addition, Ni-TMEDA@βSiO$_2$@αSiO$_2$@Fe$_3$O$_4$ was reused up to 7 times without significant loss of its activity and produced all products with high efficiency without producing any unwanted side products at room temperature.

Conflicts of interest

There are no conflicts to declare.

Acknowledgements

The authors are grateful to acknowledge the Research Council of King Saud University, Riyadh, Saudi Arabia.

References

1 R. Mozafari, F. Heidarizadeh and M. Azaroon, *RSC Adv.*, 2018, **8**, 40261–40266.
2 A. Zare, A. Kohzadian, Z. Abshirini, S. S. Sajadikhah, J. Phipps, M. Benamara and M. H. Beyzavi, *New J. Chem.*, 2019, **43**, 2247–2257.
3 H. Filian, A. Ghorbani-Choghamarani and E. Tahanpesar, *J. Iran. Chem. Soc.*, 2019, **16**, 2673–2681.
4 P. Kumar, V. Tomar, D. Kumar, R. K. Joshi and M. Nemiwal, *Tetrahedron*, 2022, **106**, 132641.
5 M. N. Chen, L. P. Mo, Z. S. Cui and Z. H. Zhang, *Curr. Opin. Green Sustain. Chem.*, 2019, **15**, 27–37.
6 M. B. Gawande, P. S. Branco and R. S. Varma, *Chem. Soc. Rev.*, 2013, **42**, 3371–3393.
7 P. Rana, R. Dixit, S. Sharma, S. Dutta, S. Yadav, B. Arora, B. Kaushik, M. B. Gawande and R. K. Sharma, *Nanoscale*, 2023, **15**, 3482–3495.
8 I. Dindarloo Inaloo, S. Majnooni, H. Eslahi and M. Esmaeilpour, *ACS Omega*, 2020, **5**, 7406–7417.
9 S. You, R. Xiao, H. Liu and M. Cai, *New J. Chem.*, 2017, **41**, 13862–13870.
10 M. Nikoorazm, A. Ghorbani-Choghamaranai, M. Khanmoradi and P. Moradi, *J. Porous Mater.*, 2018, **25**, 1831–1842.
11 P. Singh, P. Yadav, A. Mishra and S. K. Awasthi, *ACS Omega*, 2020, **5**, 4223–4232.
12 P. G. Kargar, G. Bagherzade and H. Eshghi, *RSC Adv.*, 2020, **10**, 37086–37097.
13 A. Kohzadian and A. Zare, *Res. Chem. Intermed.*, 2019, **45**, 5473–5485.
14 R. C. Cioc, E. Ruijter and R. V. A. Orru, *Green Chem.*, 2014, **16**, 2958–2975.
15 L. A. Taib and M. Keshavarz, *Polyhedron*, 2022, **213**, 115630.
16 C. Parmeggiani, C. Matassini and F. Cardona, *Green Chem.*, 2017, **19**, 2030–2050.
17 A. Yusuf, C. Snape, J. He, H. Xu, C. Liu, M. Zhao, G. Z. Chen, B. Tang, C. Wang, J. Wang and S. N. Behera, *Catal. Rev.*, 2017, **59**, 189–233.
18 Y. Wang, J. Li and Z. Wei, *J. Mater. Chem. A*, 2018, **6**, 8194–8209.
19 M. A. Abdelkareem, T. Wilberforce, K. Elsaid, E. T. Sayed, E. A. Abdelghani and A. G. Olabi, *Int. J. Hydrogen Energy*, 2021, **46**, 23529–23547.
20 B. Tahmasbi and A. Ghorbani-Choghamarani, *New J. Chem.*, 2019, **43**, 14485–14501.
21 A. Ghorbani-Choghamarani, Z. Taherinia and M. Mohammadi, *Environ. Technol. Innovat.*, 2021, **24**, 102050.
22 S. Pal, V. Chatare and M. Pal, *Curr. Org. Chem.*, 2011, **15**, 782–800.
23 A. Kohzadian, H. Filian, Z. Kordrostami, A. Zare and A. Ghorbani-Choghamarani, *Res. Chem. Intermed.*, 2020, **46**, 1941–1953.
24 H. Filian, A. Kohzadian, M. Mohammadi, A. Ghorbani-Choghamarani and A. Karami, *Appl. Organomet. Chem.*, 2020, **34**, e5579.

25 C. R. Nathaniel, R. Dhanya, P. V. Saranya and G. Anilkumar, *ChemistrySelect*, 2022, **7**, e202202763.
26 V. Kolla, A. Deyanov, F. Y. Nazmetdinov, Z. Kashina and L. Drovosekova, *Pharm. Chem. J.*, 1993, **27**, 635–636.
27 I. O. Donkor, C. L. Klein, L. Liang, N. Zhu, E. Bradley and A. M. Clark, *J. Pharm. Sci.*, 1995, **84**, 661–664.
28 J. W. Ellingboe and N. J. Princeton, *Chem. Abstr.*, 1996, **124**, 176134q.
29 K. Furukawa and T. Hasegawa, *Can. Pat. Appl.*CA 2151871, 1995; K. Furukawa and T. Hasegawa, *Chem. Abstr.*, 1996, **124**, 289568c.
30 A. Deyanov, R. K. Niyazov, F. Y. Nazmetdinov, B. Y. Syropyatov, V. Kolla and M. Konshin, *Pharm. Chem. J.*, 1991, **25**, 248–250.
31 A. Pastor, R. Alajarin, J. J. Vaquero, J. Alvarez-Builla, M. F. de Casa-Juana, C. Sunkel, J. G. Priego, I. Fonseca and J. Sanz-Aparicio, *Tetrahedron*, 1994, **50**, 8085–8098.
32 L. L. Corre, A.-L. Girard, J. Aubertin, F. Radvanyi, C. Benoist-Lasselin, A. Jonquoy, E. Mugniery, L. Legeai-Mallet, P. Busca and Y. L. Merrer, *Org. Biomol. Chem.*, 2010, **8**, 2164–2173.
33 R. K. Rawal, R. Tripathi, S. Katti, C. Pannecouque and E. De Clercq, *Bioorg. Med. Chem.*, 2007, **15**, 3134–3142.
34 A. Rosowsky, C. E. Mota and S. F. Queener, *J. Heterocycl. Chem.*, 1995, **32**, 335–340.
35 A. Monge, V. Martinez-Merino, C. Sanmartin, F. J. Fernandez, M. C. Ochoa, C. Bellver, P. Artigas and E. Fernandez-Alvarez, *Eur. J. Med. Chem.*, 1989, **24**, 209–216.
36 J. A. Kovacs, C. J. Allegra, J. C. Swan, J. C. Drake, J. E. Parrillo, B. A. Chabner and H. Masur, *Antimicrob. Agents Chemother.*, 1988, **32**, 430–433.
37 S. Trumpp-Kallmeyer, J. R. Rubin, C. Humblet, J. M. Hamby and H. D. H. Showalter, *J. Med. Chem.*, 1998, **41**, 1752–1763.
38 A. Kohzadian and A. Zare, *Silicon*, 2020, **12**, 1407–1415.
39 H. Naeimi and A. Didar, *Ultrason. Sonochem.*, 2017, **34**, 889–895.
40 H. Naeimi, A. Didar and Z. Rashid, *J. Iran. Chem. Soc.*, 2017, **14**, 377–385.
41 M. Mamaghani, L. Moslemi and A. Badrian, *Org. Chem. Res.*, 2018, **3**, 1–10.
42 H. Naeimi, V. Nejadshafiee and M. R. Islami, *Micropor. Mesopor. Mater.*, 2016, **227**, 23–30.
43 H. Naeimi and A. Didar, *J. Mol. Struct.*, 2017, **1137**, 626–633.
44 H. Naeimi, A. Didar, Z. Rashid and Z. Zahraie, *J. Antibiot.*, 2017, **70**, 845–852.
45 A. Zare, A. Kohzadian, H. Filian, M. S. Ghoreishi Nezhad and A. Karami, *Res. Chem. Intermed.*, 2022, **48**, 1631–1644.
46 M. Anbarasu, M. Anandan, E. Chinnasamy, V. Gopinath and K. Balamurugan, *Spectrochim. Acta, Part A*, 2021, **135**, 536–539.
47 A. Ghorbani-Choghamarani, B. Tahmasbi, N. Noori and S. Faryadi, *C. R. Chim.*, 2017, **20**, 132–139.
48 M. Nikoorazm, F. Ghorbani, A. Ghorbani-Choghamarani and Z. Erfani, *Appl. Organomet. Chem.*, 2018, **32**, e4282.
49 N. A. M. Barakat, B. Kim and H. Y. Kim, *J. Phys. Chem. C*, 2009, **113**, 531–536.
50 M. Esmaeilpour, A. R. Sardarian and J. Javidi, *J. Organomet. Chem.*, 2014, **749**, 233–240.
51 M. Nikoorazm, N. Noori, B. Tahmasbi and S. Faryadi, *Transit. Met. Chem.*, 2017, **42**, 469–481.
52 H. Tian, L. Pan, X. Xiao, R. W. T. Wilkins, Z. Meng and B. Huang, *Mar. Pet. Geol.*, 2013, **48**, 8–19.